UPDATED RF DESIGN AND OPTIMIZATION OF 3 GHz TRAVELING-WAVE STRUCTURES FOR THE FCC-ee HIGH-ENERGY LINAC

A. Kurtulus[1*], A. Grudiev[1], A. Latina[1], S. Bettoni[2], P. Craievich[2], J.-Y. Raguin[2]
[1]CERN, Geneva, Switzerland
[2]PSI Center for Accelerator Science and Engineering, Villigen, Switzerland

Abstract

The high-energy (HE) linac for the FCC-ee injector complex must deliver 20 GeV beams with high stability for top-up injection. Following an initial design at 2.8 GHz, the RF frequency has been updated to 3 GHz to align with the European S-band standard, enhancing compatibility with existing high-power RF components and industrial manufacturing for the Technical Design Report (TDR) phase. This paper presents the updated design of 3 m traveling-wave (TW) accelerating structures operating at 3 GHz. A parametric optimization of the full structure geometry is performed, balancing effective shunt impedance and peak surface fields. Beam-loading compensation is applied via optimized RF pulse shaping for various bunch spacings. Detailed wakefield studies are conducted for various bunch spacings to ensure the transverse wake potential remains below the stringent 0.2 V/pC/mm/m threshold. Finally, tolerance studies quantify the sensitivity of wakefield suppression to manufacturing errors, establishing practical fabrication limits for the 3 GHz structures.

INTRODUCTION AND STRUCTURE OPTIMIZATION

The FCC-ee HE-linac accelerates electrons and positrons from 2.86 GeV to 20 GeV with four bunches per RF pulse at 100 Hz, maximum 5 nC bunch charge, and nominal 25 ns bunch spacing [1]. An initial RF design at 2.8 GHz was presented in [2]. For the TDR phase, the frequency has been updated to 3 GHz (European S-band) to leverage existing RF infrastructure and simplify procurement [3]. This paper reports the updated 3 GHz design, following the same analytical methodology described in [2] (SLED pulse compressor [4] with four structures per 80 MW klystron, 14.2 MW per structure).

Using the precomputed lookup table of RF parameters described in [2] (generated from CST [5] eigenmode simulations at 5.712 GHz and scaled to 3 GHz), we performed parametric scans to satisfy beam dynamics constraints [6] for the nominal 25 ns bunch spacing:

- Phase advances per cell: 120°, 150°, 162°
- Average apertures: 0.12λ and 0.13λ
- Structure lengths: 2.5 m, 3 m, 4 m, 5 m

* adnan.kurtulus@cern.ch

Both average apertures were studied, but 0.12λ yielded a higher effective shunt impedance and is therefore presented here. The 120° phase advance provided the highest effective shunt impedance R_{eff} and lowest peak surface fields. The 3 m length was selected based on beam dynamics studies of different structure lengths [6], and is also compatible with the SwissFEL tune-free assembly process [7]. To suppress long-range transverse wakefields, tapering of the aperture radius a and iris thickness d was applied along the structure, controlled by the parameter Δ ($a_{\text{first}} = \langle a \rangle + \Delta$, $a_{\text{last}} = \langle a \rangle - \Delta$). A scan of Δ from 0 to 3 mm with a step of 0.2 mm for the nominal 25 ns spacing gave the highest $R_{\text{eff}} = 108.14$ MΩ/m at $\Delta = 1.55$ mm, but this configuration was only suitable for 25 ns spacing.

To enable operation with different bunch spacings (5, 10, 15, 20, 25, 30, 40, and 50 ns), we fine-tuned Δ to 1.4 mm, achieving $R_{\text{eff}} = 107.24$ MΩ/m (a 0.83 % decrease from the $\Delta = 1.55$ mm case). The final optimized 3 GHz structure achieves a loaded accelerating voltage of 66.64 MV and a loaded average gradient of 22.21 MV/m for four-bunch operation at 25 ns spacing. This configuration satisfies the wakefield criteria for multiple spacings, as demonstrated in the next section. The complete structure parameters are summarized in Table 1.

Table 1: Optimized 3 GHz Structure Parameters (3 m Length, $\langle a \rangle = 0.12\lambda$)

Parameter	Value	Unit
Frequency	3	GHz
Δ	1.4	mm
Number of cells	90	–
Aperture (first/last)	13.39/10.59	mm
Iris thickness (first/last)	2.30/3.50	mm
v_g/c (first/last)	3.66/1.50	%
R'/Q (first/last)	4.01/4.62	kΩ/m
Q (first/last)	16121/15733	–
Filling time	430	ns
SLED coupling	15	–
R_{eff}	107.24	MΩ/m
Klystron power per structure	14.2	MW
V_{acc} (loaded)	66.64	MV
G_{avg} (loaded)	22.21	MV/m
$E_{s,\text{max}}$	79	MV/m
$S_{c,\text{max}}$	624	mW/mm^2

WAKEFIELD STUDIES

Transverse wakefields were calculated using the dipole higher-order mode (HOM) data from the lookup table, following the method described in [2]. To provide a more realistic prediction, we also employed the ECHO2D time-domain solver [8], which models all 90 cells and accounts for an infinite number of HOMs as well as cell-to-cell coupling.

The $\Delta = 1.55$ mm configuration, which maximized R_{eff} for 25 ns spacing, did not position the wake potential notches at the desired bunch locations. By fine-tuning Δ to 1.4 mm, we aligned the notches of the envelope-of-the-envelope wake potential with the bunch positions for spacings of 10, 15, 20, 25, 30, 40, and 50 ns. Looking at the more realistic ECHO2D results, bunch spacings of 10 ns and above satisfy the wakefield constraint $W_t < 0.2$ V/pC/mm/m [6], while 5 ns spacing exceeds the limit and is therefore not feasible.

Figure 1 shows the envelope-of-the-envelope transverse wake potential up to 150 ns calculated with both methods: the analytical wake function from the lookup table (red trace) and the ECHO2D solver (green trace). The vertical dashed blue lines indicate the bunch locations for the studied bunch spacings: 5, 10, 15, 20, 25, 30, 40, and 50 ns.

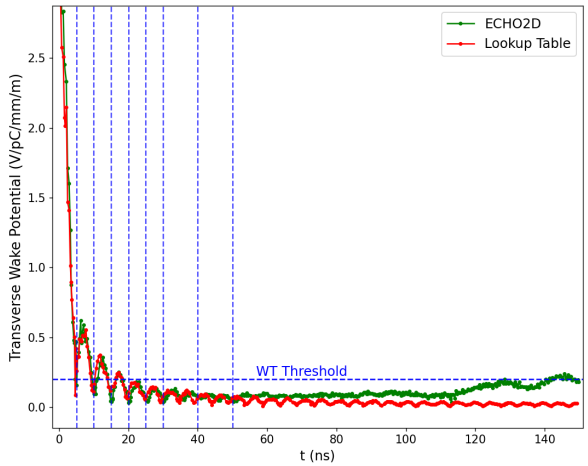

Figure 1: Envelope-of-the-envelope transverse wake potential W_t vs. time (red: analytical, green: ECHO2D). Vertical dashed blue lines indicate the bunch locations for the studied bunch spacings.

BEAM-LOADING STUDIES

For multi-bunch operation, beam-loading causes a time-dependent reduction in the accelerating gradient, leading to bunch-to-bunch energy spread. Using the dynamic RF pulse-shaping method described in [2], we performed bunch-to-bunch energy minimization by reshaping the RF input pulse for different bunch spacings.

Figure 2 shows the unloaded and loaded gradient profiles after optimization of the RF input pulse for the nominal 25 ns spacing. The four red dots indicate the positions of the bunches, and the corresponding loaded accelerating voltages they experience result in a bunch-to-bunch energy spread of 0.05 %.

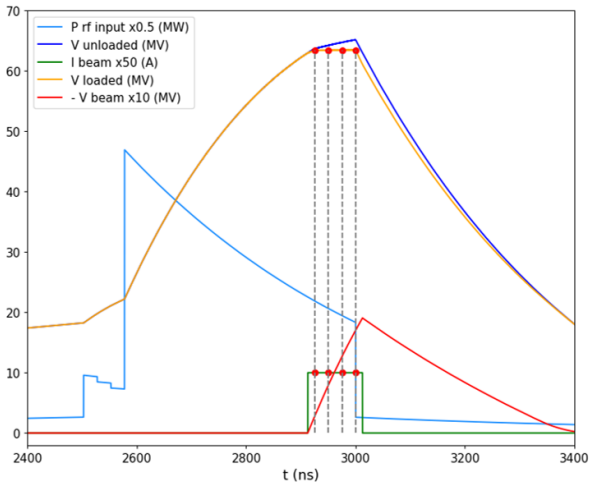

Figure 2: Unloaded and loaded gradients for four-bunch operation at 25 ns spacing. The red dots indicate the bunch positions.

The beam-loading effect is evaluated by normalizing the beam voltage to the maximum unloaded voltage, as shown in Fig. 3. The fourth bunch experiences the largest beam-loading effect, with an observed variation of approximately 2.76 %.

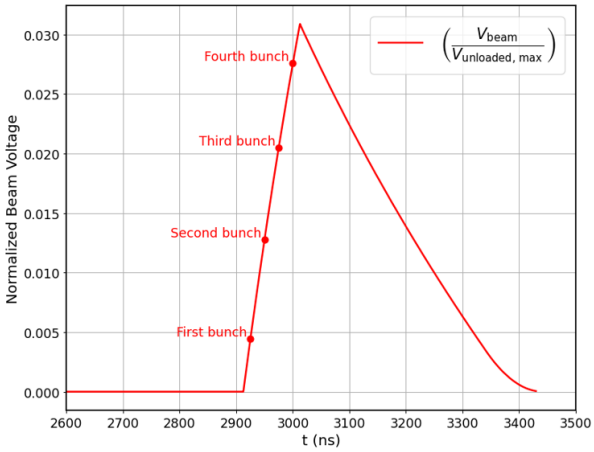

Figure 3: Distribution of the beam voltage for the four bunches, normalized to the maximum unloaded voltage.

The results above assume a nominal bunch charge of 5 nC. However, top-up operation requires handling arbitrary charge distributions across the four bunches. Using the same $\Delta = 1.4$ mm structure, we adopt the "golden pulse" approach [2], averaging the optimized RF pulses for unloaded and fully loaded beams. This limits the bunch-to-bunch energy spread to ± 1.17 %, demonstrating that the fine-tuned structure maintains good performance even under dynamically varying charge configurations.

We extended the same beam-loading compensation procedure to the bunch spacings that satisfy the wakefield constraint (10, 15, 20, 25, 30, 40, and 50 ns). For each spacing, the RF input pulse was re-optimized to minimize the bunch-to-bunch energy spread. Table 2 summarizes the

resulting loaded accelerating voltage and bunch-to-bunch energy spread within four bunches for each configuration.

Table 2: Beam-loading Compensation Results for Different Bunch Spacings

Bunch spacing (ns)	Loaded V_{acc} (MV)	Energy spread (%)
10	68.21	0.66
15	67.79	0.03
20	67.17	0.07
25	66.64	0.05
30	66.18	0.07
40	64.99	0.06
50	63.72	0.05

As the bunch spacing increases, the required RF pulse length becomes longer, which gradually reduces the maximum achievable loaded accelerating voltage. For the 10 ns spacing, the beam-loading compensation approaches the practical limit of the RF pulse-shaping technique, resulting in an energy spread of 0.66 %. Nevertheless, this value remains within the ±1.17 % margin of the golden pulse, confirming that 10 ns operation is feasible for top-up injection with the fine-tuned structure.

TOLERANCE STUDIES

The transverse wakefield is dominated by the first dipole HOM. Using CST's eigenmode solver, we computed the synchronous phase and the corresponding dipole frequency of the first dipole mode for the first, middle, and last cells of the fine-tuned $\Delta = 1.4$ mm structure. To assess manufacturing tolerances, we performed a sensitivity analysis by varying three critical geometric parameters: cavity radius (R_c), aperture radius (a), and iris thickness (d), independently from −5 to +5 µm in 1 µm steps, corresponding to the expected machining precision.

The sensitivity study revealed that the last cell is the most sensitive to parameter variations. Among the three parameters, R_c exhibits the highest sensitivity, with a dipole frequency shift of 0.1 MHz/µm. Figure 4 shows the dipole frequency shift as a function of each parameter variation for the last cell. Using these frequency shifts, we reconstructed the transverse wakefield by interpolating the dipole mode frequencies along the structure between the first, middle, and last cells. The resulting wakefield deviation from the original fine-tuned configuration was found to be negligible, confirming that the expected manufacturing tolerances are acceptable for preserving wakefield suppression performance.

To further assess the impact of manufacturing tolerances, parameter deviations up to 50 µm were also considered. These studies evaluated the effects on wakefield stability and frequency shifts, with particular attention to the operational bunch spacing locations (10, 15, 20, and 25 ns). Deviations up to 50 µm produced no significant changes, with R_c consistently having the largest impact as expected. Based on these comprehensive results, a tolerance limit of ±10 µm is recommended for precision fabrication and quality control of the 3 GHz structures..

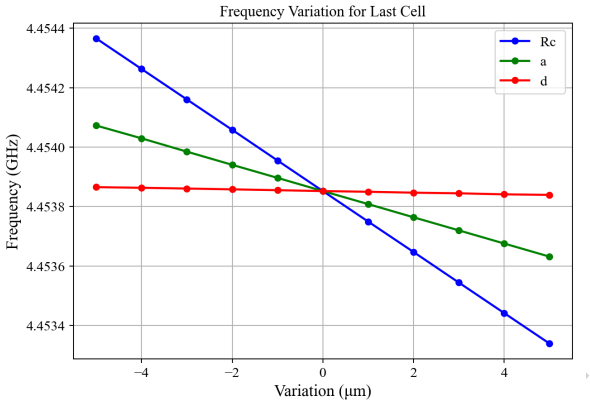

Figure 4: Dipole frequency shift of the first dipole mode as a function of geometric parameter variations (R_c, a, d) for the last cell.

CONCLUSION

This paper presented the updated design of 3 m traveling-wave accelerating structures at 3 GHz, following the same analytical methodology as the initial design.

A parametric optimization of the structure geometry selected the 120° phase advance, 0.12λ average aperture, and 3 m length as the baseline. The tapering parameter Δ was fine-tuned from 1.55 mm (optimal for 25 ns only, R_{eff} = 108.14 MΩ/m) to 1.4 mm, achieving R_{eff} = 107.24 MΩ/m (a 0.83 % decrease) while enabling operation with multiple bunch spacings (10, 15, 20, 25, 30, 40, and 50 ns). The final structure delivers a loaded voltage of 66.64 MV and a loaded average gradient of 22.21 MV/m at 25 ns spacing.

Wakefield studies confirmed that the $\Delta = 1.4$ mm configuration satisfies the $W_t < 0.2$ V/pC/mm/m threshold for all spacings ≥ 10 ns, with 5 ns being infeasible. Beam-loading compensation reduced the energy spread to 0.05 % at 25 ns spacing and 0.66 % at the challenging 10 ns spacing, the latter remaining within the ±1.17 % golden pulse margin for top-up operation. Tolerance studies identified the cavity radius as the most sensitive parameter (0.1 MHz/µm) and recommend a ±10 µm fabrication limit.

The updated 3 GHz design provides a robust, manufacturable baseline for the FCC-ee HE-linac, supporting flexible bunch spacing operation while maintaining high RF efficiency, effective wakefield suppression, and beam-loading compensation for top-up injection.

ACKNOWLEDGEMENTS

The authors would like to express their gratitude to the Swiss Accelerator Research and Technology (CHART) for financing the FCC-ee injector design study effort.

REFERENCES

[1] P. Craievich, "Injector complex: status and outlook", unpublished, FCC Week 2024, San Francisco, United States, 2024, https://indico.cern.ch/event/1298458/contributions/5977869/,

[2] A. Kurtulus, A. Grudiev, A. Latina, S. Bettoni, P. Craievich, and J.-Y. Raguin, "RF design and optimization of the high-energy linac for the FCC-ee injector complex", *Phys. Rev. Accel. Beams*, p. 101601, Aug. 2025. doi:10.1103/x2rz-2qxj

[3] A. Grudiev and other, "FCC-ee injector linacs: design and rf frequency choices for the tdr", Presentation at FCC Week 2025, May 2025, https://indico.cern.ch/event/1408515/contributions/6515052/attachments/3072060/5435058/FCCweek2025_Grudiev.pdf,

[4] Z. Farkas, H. Hogg, G. Loew, and P. B. Wilson, "Sled: a method of doubling slac's energy", in *Proc. of 9th Int. Conf. on High Energy Accelerators, SLAC*, p. 576, 1974.

[5] CST Studio Suite, Dassault Systèmes, 2024. https://www.3ds.com/products-services/simulia/products/cst-studio-suite/

[6] S. Bettoni *et al.*, "Beam dynamics optimization of the high energy linac of the FCCee injector", presented at IPAC'26, Deauville, France, May 2026, paper WEP5054, this conference.

[7] U. Ellenberger *et al.*, "Status of the manufacturing process for the swissfel c-band accelerating structures", in *Proceedings of the 35th International Free-Electron Laser Conference (FEL2013)*, pp. 245–249, 2013. https://accelconf.web.cern.ch/fel2013/papers/tupso17.pdf

[8] I. Zagorodnov, K. L. Bane, and G. Stupakov, "Calculation of wakefields in 2d rectangular structures", *Phys. Rev. Spec. Top. Accel. Beams*, vol. 18, no. 10, p. 104401, 2015. doi:10.1103/PhysRevSTAB.18.104401